Phase behaviour during electrochemical cycling of Ni-rich cathode materials for Li-ion batteries

Chao Xu, Philip J. Reeves, Quentin Jacquet, and Clare P. Grey*

Dr. C. Xu, Dr. P. J. Reeves, Dr. Q. Jacquet, Prof. C. P. Grey
Department of Chemistry, University of Cambridge, Cambridge, CB2 1EW, United Kingdom

E-mail: cpg27@cam.ac.uk

Dr. C. Xu, Dr. P. J. Reeves, Dr. Q. Jacquet, Prof. C. P. Grey
The Faraday Institution, Quad One, Harwell Science and Innovation Campus, Didcot, OX11 0RA, United Kingdom

Although layered lithium nickel-rich oxides have become the state-of-the-art cathode materials for lithium-ion batteries in EV applications, they can suffer from rapid performance failure – particularly when operated under conditions of stress (temperature, high voltage), the underlying mechanisms of which are not fully understood. In this essay, we aim to connect the electrochemical performance with changes in structure during cycling. First, we compare the structural properties of $LiNiO_2$, to the substituted Ni-rich compounds NMCs ($LiNi_xMn_yCo_{1-x-y}O_2$) and NCAs ($LiNi_xCo_yAl_{1-x-y}O_2$). Particular emphasis is placed on decoupling intrinsic behaviour and extrinsic "two-phases" reactions observed during initial cycles, as well as after extensive cycling for NMC and NCA cathodes. We highlight the need to revisit the various high-voltage structural change processes that occur in $LiNiO_2$ with modern characterization tools to aid the understanding of the accelerated degradation for Ni-rich cathodes at high voltages.

1. Introduction

The widespread deployment of electric vehicles (EVs), powered by rechargeable lithium-ion batteries (LIBs), represents a much needed opportunity to reduce fossil fuel consumption massively and CO_2 emission in the transportation sector.[1–3] The state-of-the-art cathodes for EV Li-ion batteries are a family of materials derived from layered $LiNiO_2$ (LNO) by substitution of Ni with elements such as Mn, Co and Al. The two resulting subgroups are known as Ni-rich NMC ($LiNi_xMn_yCo_{1-x-y}O_2$, $x \geq 0.5$) and NCA ($LiNi_xCo_yAl_{1-x-y}O_2$, $x \geq 0.5$).[4,5] Their parent material, $LiNiO_2$, was explored as a promising Li-ion cathode in the 1990s as it can offer substantially higher practical capacities than the canonical $LiCoO_2$ at a lower voltage.[6–9] Compared to $LiCoO_2$, another attractive property of $LiNiO_2$-based materials is that they require a substantially lower amount of the more costly mineral cobalt, which is found in fewer places globally with much lower reserves and production levels.[10,11] Thus, there are good reasons to adopt Ni-rich based batteries chemistries for EV applications; however, these cathode materials typically show faster performance fading compared to both $LiCoO_2$ and their lower Ni-content analogues, and the fundamental mechanisms causing this are still not fully understood.[4,5]

A battery material's redox potential, capacity and cycle life, are strongly coupled to the evolution of their structural properties during the electrochemical reaction.[12] Li removal (or insertion) can occur by two different thermodynamic mechanisms: i) a solid-solution reaction, corresponding to a continuous change of the crystal structure, or ii) a two-phase reaction during which either a new Li-poor (or Li-rich) phase nucleates and grows. Both mechanisms can have very different consequences on the homogeneity of the electrochemical reaction. Phase transitions in two-phase reactions are intrinsically accompanied by a free-energy barrier due to the coherency strain energy and interfacial energy between the two phases.[13] This will result in a measurable voltage hysteresis, which may become larger at faster lithiation/delithiation rates, leading to a reduction in the reversible capacity (in a fixed voltage

window) and energy efficiency.[14] Moreover, the free-energy barrier can also lead to a non-uniform current distribution across different electrode particles, and consequently, individual particles can experience a much higher current density than that set by the total current of the electrode, as recently demonstrated in $LiFePO_4$.[15,16] The Li insertion mechanism also has consequences for the mechanical integrity of the particles. For a solid-solution reaction, a Li concentration gradient inside a particle can build up, causing stress and strain, and eventually crack formation, particularly in cases were the Li removal/insertion of Li causes drastic lattice expansion or contraction and at high rates. Such mechanical degradation is generally thought to be more pronounced in two-phase reactions as there is stress and strain at the interface between the two phases and if, similar to the solid-solution case, the lattice parameter difference between the phases is large, cracking can occur. Two-phase reactions, by their nature, produce phase boundaries inside the particles, and the rate is then determined by the rate of nucleation and then movement of the phase boundary. Finally, irreversible phase transformation to structures which have different electrochemical properties, can result in a direct loss of active material and therefore capacity fading. For instance, layered $LiMnO_2$ undergoes a phase transformation to a disordered and then more ordered spinel structure, resulting in large irreversible capacity loss.[17] In light of the influence of the structural evolution on the cell performance, it is crucial to develop an in-depth understanding of the structures of the Ni-rich materials as well as how they change during battery cycling.

The purpose of this essay is to critically review recent progresses in the bulk phase behaviour of state-of-the-art layered Ni-rich cathode materials during cycling, and to push the understanding of the structure-driven degradation mechanisms. This review starts with a description of the fundamental structural properties of the parent compound $LiNiO_2$, which serves as a baseline for the discussion on the intrinsic phase behaviour of the state-of-the-art NMC and NCA (Ni ≤ 80 %) materials. The last two sections review the apparent "two-phase" processes in Ni-rich lithium transition metal oxides ($LiTMO_2$s), first, during their initial

cycles and second, after extensive electrochemical ageing. We acknowledge that there are other important structural aspects of Ni-rich materials, such as structure transformations under thermal stress or approaches to further improve structural stabilities by doping, controlling morphology or producing gradient structures, that are not addressed in this essay but more details can be found in the literature.[12,18–20]

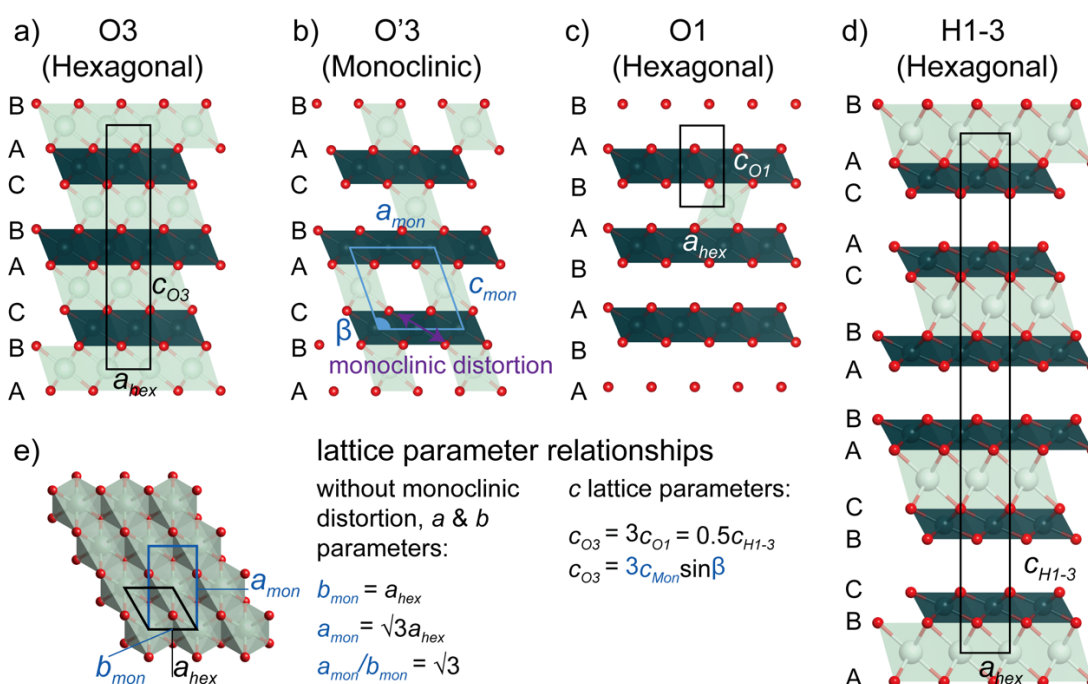## 2. The crystal chemistry of layered transition lithium metal oxides

Figure 1. Illustrations of crystal structures relevant to the layered Ni-rich cathodes. a-d) Views parallel to the layer direction highlight the different stacking regimes and are labelled using Delmas's notation and the crystallographic family they belong to (in brackets). The oxygen planes are labelled to indicate their stacking sequences. e) shows the view perpendicular to the layer direction highlighting the relationship between the hexagonal and monoclinic unit cells; if there is no monoclinic distortion $a_{mon}/b_{mon} = \sqrt{3}$. Relationships between the c lattices of (a-d) are also given. Unit cells are shown in black (hexagonal) or blue (monoclinic) and Li, TM and O atoms in light green, dark green and red respectively.

Figure 1a shows the typical O3 structure (space group $R\bar{3}m$) which has an *fcc* oxygen framework with a *AB CA BC* stacking sequence, the TM ions and Li ions occupying the alternating layers.[21] The "O" in O3 denotes the octahedral coordination environment of the alkaline cation, i.e. lithium in the present case, and the number "3" represents the number of

4

TMO$_2$ slabs in the unit cell. Distorted O3 structures associated with a symmetry lowering from $R\bar{3}m$ to monoclinic C2/m are often observed for layered cathodes due to lithium/vacancy ordering and/or collective Jahn-Teller distortion. Such monoclinic phases (M) are also referred to as O'3 (Figure 1b) to distinguish them from the undistorted O3 $R\bar{3}m$ structure, while illustrating that the O3 stacking is preserved. Another important structure for the phases discussed here is the O1 structure (space group $P\bar{3}m1$) which is characterised by the $AB\ AB$ stacked oxygen layers (i.e. one TMO$_2$ slab in the unit cell), as shown in Figure 1c.[21] In addition to these ideal O3 and O1 structures, hybrid H1-3 structures comprising alternating O1 and O3 blocks, are also observed in layered transition metal oxides (Figure 1d).[22–24] As a specific example, this H1-3 phase is observed for Li$_x$CoO$_2$ at ~4.6 V vs. Li, and further delithiation of this phase leads to another phase transformation to the O1 structure (Figure 1c).[22–24] The relationships of the lattice parameters between these structures are also given in Figure 1e.

The majority of phase transformations in LiTMO$_2$s occur without a change in stacking sequence (i.e. O3 stacking preserved), which has led to a second notation used to describe the phase transformations. In this system, phases are labelled by a letter, which gives information about the symmetry of the unit cell, and number, which denotes the order in which each phase of that symmetry, is observed on charge. In this notation, structures in the rhombohedral lattice system are usually denoted as "H" (hexagonal) rather than "R"; they are typically expressed in the hexagonal lattice setting, with the layers in the ab plane and the c direction perpendicular to the layers (Figure 1a). This means that the $R\bar{3}m$ structures of pristine LiNiO$_2$, NMC, NCA *etc.* are denoted as "H1", the next (second) phase observed in the hexagonal crystal family on delithiation would be "H2" etc. The sequence of phases observed for LiNiO$_2$, discussed in detail in section below, is H1→M→H2→H3 with all phases having an O3 stacking sequence.

Ni-rich LiTMO$_2$s adopt the typical O3 structure in their fully lithiated state; however, instead of the ideal scenario where the TM ions and Li-ions occupy alternating layers, LiNiO$_2$ (as well as its NMC and NCA analogous) often exhibits antisite defects such that a measurable amount of Ni^{2+} is present in the Li layer.[25] This has often been attributed to the similar ionic radius of the Li$^+$ (0.76 Å) and Ni^{2+} (0.69 Å). Two scenarios are possible. The first results in off-stoichiometric materials typically denoted as $Li_{1-z}Ni_{1+z}O_2$, or $[Li_{1-z}Ni_z^{2+}]_{3b}[Ni_z^{2+}Ni_{1-z}^{3+}]_{3a}O_2$ (Li occupies 3b sites and Ni occupies 3a sites), which will be favored or be driven by Li loss. Alternatively, the material remains stoichiometric and forms paired antisite defects, i.e., z amount of Li occupying Ni sites.[26] In practice, both of the two possibilities are likely to occur depending on, for instance, the sample stoichiometry, synthesis conditions and the addition of additional TMs beyond Ni. To facilitate discussion, the term "antisite defects" is used in this essay to denote Ni^{2+} occupies the 3b sites. The amount of antisite defects has a profound impact on nearly all of the properties of LiNiO$_2$ and its derivatives, ranging from electrochemical performance, electronic and magnetic characteristics, as well as phase behaviours.[27] The variation in the amount of antisite defects, as a result of different synthesis conditions, is one source of the many discrepancies in the literature, and therefore careful characterization is of great importance to the understanding of the Ni-rich cathode materials.

3. Structural evolution during cycling of the parent material – LiNiO$_2$

To discuss the intrinsic phase behaviour of LNO, we chose a recent report by de Biasi *et al*. as their $Li_{1-z}Ni_{1+z}O_2$ material has a minimal antisite defect concentration of ~1% and the structure change during lithiation/delithiation was carefully characterized by *operando* PXRD (shown in Figure 2a).[28]
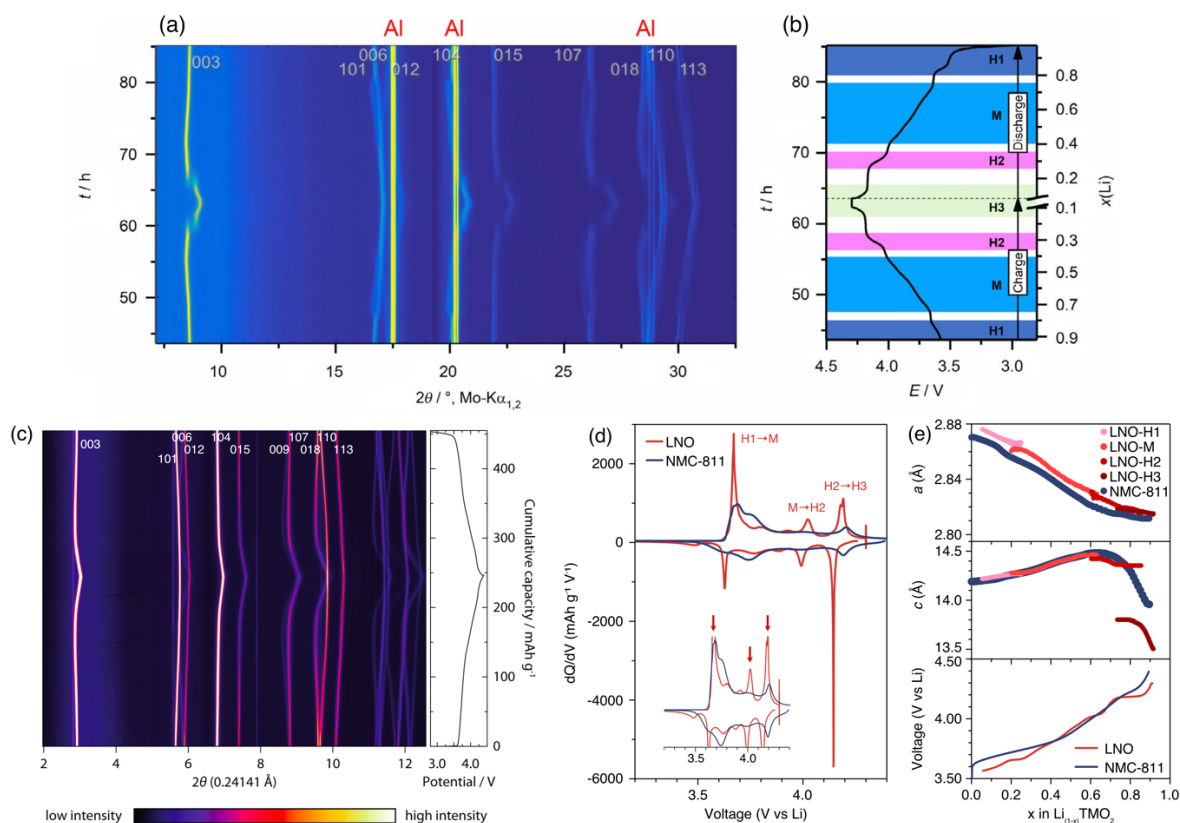
6

Figure 2. Intrinsic structure evolution of LiNiO₂ and NMC-811. a,b) *operando* X-ray diffraction results (a) of LNO during galvanostatic cycling and the corresponding voltage profile (b). c) Synchrotron radiation *operando* X-ray diffraction results of NMC-811 during galvanostatic cycling and the corresponding voltage profile. d) Comparison of the LNO and NMC-811 dQ/dV profiles. Inset in (d) represents magnified data and the arrows from low to high voltages indicate the dQ/dV peaks which correspond to the H1→M, M→H2 and H2→H3 transitions in LNO, respectively. e) Comparison of the lattice parameters and voltage profiles of LNO and NMC-811. Panels (a,b) reproduced with permission from reference.[28] Copyright 2019 Wiley-VCH. Panels (c) reproduced with permission from reference.[29] Copyright 2019 American Chemical Society. The LNO data in (d,e) courtesy of L. de Biasi.

The diffraction results reveal that the material follows a sequence of phase transitions:

H1→M→H2→H3 which correlates with the multiple plateaus observed in the voltage profile up to 4.3 V vs Li (Figure 2b). Note that further charging beyond 4.3 V results in rapid increase in the voltage with a very limited amount of lithium being extracted, and voltage profiles with higher cut-off voltages are available in reference[30,31]. In detail, upon charge, pristine $Li_{0.99}Ni_{1.01}O_2$ first undergoes a solid-solution reaction until ~$Li_{0.8}Ni_{1.01}O_2$, after which it exhibits a phase transformation from a hexagonal (H1 phase) to a monoclinic structure (M phase). This transition is clearly evidenced by the splitting of multiple reflections, e.g.

$(101)_{hex}$ at ~17° 2θ (Figure 2a; note Mo radiation used in this diffraction study). The material maintains its monoclinic symmetry on further delithiation until ~$Li_{0.4}Ni_{1.01}O_2$. Then, it exhibits another phase transformation namely M to H2 between x = 0.40 and 0.36 (x represents the lithium content, i.e. Li_xTMO_2). The H2 phase remains until x = 0.26. Finally, the state of charge (SoC) range of x = 0.26 to 0.16 is associated with the first order H2-H3 transition at ~4.2 V vs. Li as deduced from the appearance of a new (003) reflection at around 8°. It should be noted that discrepancies in the details, for instance, at what SoCs these transitions occur, exist in the current literature, and this is likely to be associated with the different amount of antisite defects and possibly differences in cycling conditions and electrode fabrication.[27,28,31–33]

The Rietveld refinement against these patterns allows the cell parameter evolution to be followed, the cell parameters having been converted into those of the corresponding hexagonal unit cell to facilitate comparison (see ref[28] for details of the conversion). a_{hex} decreases monotonically during the entire delithiation which is attributed to a contraction in the NiO_6 octahedra due to the oxidation of Ni^{3+} to Ni^{4+}. The c_{hex} parameter follows a more complex behaviour. During the course of the H1→M→H2 transitions (0.26 < x < 1), c_{hex} gradually increases but then starts to decrease from x ≈ 0.4. Upon further delithiation corresponding to the H2→H3 transition (0.26 < x < 0.16) a sharp decrease of c_{hex} is observed, going from ~14.4 Å in H2 to values ranging from ~13.8 Å[28], ~13.6 Å[31] to even ~13.4 Å[33] in H3, depending on the reports. This difference is most likely due to different antisite defects in the pristine material, the Ni present in the Li layers preventing complete collapse of the layers. The initial increase of c_{hex} is due to the increased O-O electrostatic repulsion as a result of the removal of screening Li ions from the interlayer; the decrease at high SoCs is however less definitive; the current theory is that at high SoCs, the Ni-O bond becomes more covalent, reducing the electrostatic repulsion between the O anions and causing the Li-layer to contract.[27,34]

8

As LNO approaches the fully delithiated state, another first-order phase transition was reported by Croguennec et al. during which the structure changes from the H3 phase (O3 layer stacking) to another hexagonal phase (H4) which features an O1 stacking sequence (more accurately a non-ideal O1 structure with the presence of O3-type stacking faults).[30,35] Interestingly, this non-ideal O1 phase was obtained under two separate conditions, both involving extremely slow charging to either 4.2 V or 4.45 V *vs* Li (~200-300 h potentiostat charging at a rate of 10 mV/4h with additional hundreds of hours voltage hold);[30,34,35] this phase transition was not observed under standard galvanostatic charging up to 4.3 V vs. Li at a rate of C/20,[28] or to 4.6 V vs. Li at a rate of C/100,[31] despite the fact that these *operando* PXRD experiments were conducted using modern equipment should be more sensitive to small structural changes. This H3→H4, transition is fundamentally different from the other phase changes in $LiNiO_2$, which are observed under normal charging conditions and do not cause a stacking sequence change. To emphasize these differences, it will be referred to as H3→H4(O1) in this essay.

Having given a description of the unit cell evolution, we now focus on the exact structures of the different phases appearing during delithiation with the aim to understand the energetics behind there formation.

3.1 The origins of monoclinic distortion

The lowering in symmetry, i.e. from hexagonal to monoclinic, which occurs for Li_xTMO_2 compositions from x ≈ 0.8 to 0.4, was originally proposed to stem from a collective Jahn-Teller (JT) distortion due to the presence of JT active Ni^{3+} (valance electronic configuration of $t_{2g}^6 e_g^1$).[36] The fact that a collective JT distortion causes a monoclinic distortion in partially delithiated materials but not in the pristine material, which contains more JT active Ni^{3+} ions[25,28,31,33] is initially puzzling. This peculiar behavior was explained with evidence from electron diffraction,[37] as well as first-principles calculations,[38–41] which revealed that a monoclinic distortion can be caused by the synergistic effects of a lithium/vacancy ordering

coupled with a cooperative JT distortion. Such lithium/vacancy-ordered phases are stabilized by both the short-ranged, repulsive, in-plane Li-Li interactions, as well as the long-ranged, inter-plane 180° Li_A–O–TM–O–Li_B chain with a JT-active Ni^{3+} center.[38,41] The latter is attributed to the fact that this configuration lowers the energy of anti-bonding e_g^* orbitals due to the hybridization of Li-$2s$ and O-$2p$ orbitals, which allows the e_g^* orbitals to be preferentially filled, resulting in charge localization and hence enhanced JT effects.[38,41] Based on the first-principles calculations, Arroyo y de Dompablo et al. predicted a number of ordered phases at x = 0.75, 0.5, 0.4, 0.33 and 0.25, among which $Li_{0.75}NiO_2$ and $Li_{0.4}NiO_2$ are the two particularly high in monoclinicity (i.e. the ratio between the a and b monoclinic lattice parameters, a_m/b_m, which is a measure of structure deviation from the rhombohedral symmetry is largest; for an undistorted rhombohedral lattice, the value is $\sqrt{3}$ (Figure 1e)).[41] A JT-mediated lithium/vacancy ordering is supported by solid-state nuclear magnetic resonance (ssNMR) spectroscopy. The ^7Li NMR shifts of Li_xNiO_2 phases are dominated by the Fermi-contact interaction, the through-bond interaction of unpaired electrons (here on Ni^{3+} in Li_xNiO_2) with the nuclear spin of interest ($^{6/7}Li$).[42] In pristine LNO, the lack of a monoclinic distortion, is consistent with $^{6/7}Li$ NMR measurements, which can be modelled on the basis of a dynamically averaged JT distortion.[43] For LNO samples in monoclinic regime (0.4 ≤ x ≤ 0.75), Chazel et al. showed, using empirically derived Fermi-contact shifts for Ni^{3+},[44] that the observed Li spectra were consistent with the x = 0.5 and x = 0.25 structures predicted by Arroyo y de Dompablo.[40,45] A precise assignment of which vacancy ordering dominates is challenging. This is because the observed NMR shifts can be explained by either Li, coordinated by $6Ni^{3+}$ next nearest neighbours (as was suggested by Chazel et al.) or by a cooperative JT distortion, in which each Li is coordinated by for two JT lengthened $Ni^{3+}(e_g*)$–O–Li bonds. This is because the JT distortion localizes the unpaired electrons in e_g^* orbitals, therefore the magnitude of the Li shifts are highly sensitive to the orientation of the

lengthened JT axis.[43] During the monoclinic region, it is likely the Li shift is caused by static, cooperative JT distortion.

After the wide monoclinic regime ($0.4 \leq x \leq 0.75$), Li_xNiO_2 returns back to the original O3 $R\bar{3}m$ structure, this phase is denoted H2. Surprisingly, the Li NMR shift remains large into the H2 region (x = 0.25),[45] suggesting Li is still preferentially coordinated by Ni^{3+} in its next nearest neighbour shell, despite the lack of a cooperative JT distortion. The absence of a cooperative distortion for $x \leq 0.4$, despite the apparent preference of Li to reside in specific environments, is likely caused by the lack of Ni^{3+} required to form the extended chains of $Li_A–O–TM–O–Li_B$ bonds, which are required to drive the cooperative JT distortion in the monoclinic region. The phase transition M→H2 takes place over a narrow two-phase region (approximately $0.36 \leq x \leq 0.40$) and is accompanied by a small decrease in the c-lattice parameter.

3.2 H2 to H3 transition.

The H3 phase, having a substantially smaller c parameter compared to the H2, forms through a biphasic process despite the energetically costly and highly strained H3/H2 interface. This raises the question of the origin of the thermodynamic driving force for the phase separation. A similar two-phase reaction, associated with a drastic collapse in the interlayer distance, is the phase transformation from O3 to H1-3 observed for Li_xCoO_2 at ~4.6 V vs. Li.[22–24] H1-3 structured Li_xCoO_2 gives rise to several Bragg peaks at positions which are clearly distinguishable from the O3 structure, for instance the (003) peak at ~10º and (009) at ~32º (2θ values, CuKα radiation).[22,24] Such signatures, however, to the best of our knowledge, have never been reported for LNO, suggesting that H3 is unlikely to be an H1-3 structure. O1-type stacking faults could also occur in a less ordered manner so that no long-range ordering and hence no distinct Bragg peaks can be observed. This will, however, lead to the broadening of ($h0l$) and ($0kl$) reflections (for instance, (101)), as shown by a simulation of the diffraction pattern of the O3 structure with randomly distributed O1-type stacking faults by

Croguennec et al.[34] However, recent *operando* diffraction results show no obvious broadening of the (101) reflection.[28,31] Therefore, it is reasonable to conclude that the stacking sequence of the H3 LiNiO$_2$ phase remains O3.

Another possibility is that H3, similar to the M phase, has distinct lithium/vacancy ordering which confers additional stability; however, to the best of our knowledge, there is no direct experimental and/or simulation evidence in the current literature to support this hypothesis hence calling for further characterization of this high state of charge phase.

3.3 H3→H4(O1) transition

The H3→H4(O1) transition has been observed for LNO on charging to both 4.2 V and 4.45 V suggesting that the voltage threshold of this transition is at or below 4.2 V vs. Li.[30] However, the kinetics of this transition in LNO must be very sluggish, as it is only observed under extremely slow charging in LNO samples with low amounts of antisite defects. The presence of Ni in the Li layer may hinder complete delithiation of the layers and therefore also prevent a change in the stacking sequence. Indeed, for samples with an antisite defect concentration greater than 7%, the H3→H4(O1) transition in LNO can no longer be observed.[35]

The H3→H4(O1) transition observed in LNO should be compared to the H1-3 to O1 transition observed in Li$_x$CoO$_2$ at high SoCs which is also featured with a change in the stacking sequence. First-principles calculations for CoO$_2$ have shown that the O1 stacking is thermodynamically more stable than the O3 by 40 meV/m.f., which is attributed to the minimization of the overlap between the oxygen *p* orbitals from two adjacent metal oxide sheets in the O1 stacking sequence.[34,38] However, for NiO$_2$ the O1 stacking is only marginally lower in energy than the O3 stacking (7 meV/m.f., which is comparable to the intrinsic DFT errors). Thus, due to a combination of lower thermodynamic driving force, sluggish kinetics, and the presence of antisite defects, O1 structured NiO$_2$/Li$_x$NiO$_2$ is only rarely observed. It is worth noting that the formation of O1 phase, particularly by extremely

slow charging and chemical delithiation, could potentially be an artifact due to proton insertion which can assist the stacking sequence change.[46,47]

4. Intrinsic phase behavior of Ni-rich materials

Having described the structural evolution of LNO, we now focus on the NMC and NCA materials. The voltage features associated with the various phase transitions in LNO are substantially weaker but discernible in NMC-811 ($LiNi_{0.8}Mn_{0.1}Co_{0.1}O_2$) as shown in the differential voltage profiles in Figure 2d, indicating that NMC-811 may feature similar structural transformations. However, recent *operando* diffraction results performed during the 1st cycle of a high-quality commercial NMC-811 with a low amount of antisite defects (~1%) (Figure 2c) shows that this is not the case. In sharp contrast to the LNO results, which show that various peak splitting (Figure 2a), all peaks of the NMC-811 (except for the (110) peak which will be discussed in detail in the section 6.1) material show continuous shifts with no obvious splitting. As a result, the patterns can be fitted with one $R\overline{3}m$ phase throughout the cycling (up to 4.8 V vs. Li) as demonstrated in numerous studies.[29,48,49] The extracted cell parameter evolution is generally similar to the LNO: upon delithiation, a_{hex} continuously decreases and c_{hex} increases initially but then decreases rapidly as shown in Figure 2e. One distinct difference lies in the *c*-parameter. For the LNO, the rapid contraction happens *via* the H2-H3 transition during which the *c*-parameters of both the H2 and the H3 phases remain relatively constant with that of the H3 being considerably smaller (Figure 2e). By contrast, for NCAs and NMCs, the change in the *c*-parameters is continuous.[29,49,50] Of note, the onset of the *c*-parameter collapse is heralded by high voltage peaks in the dQ/dV plots, which some authors have assigned to an H2-H3 transformation.[51–53] At this stage, we stress that electrochemical features cannot be used independently to assign certain phase transformations and should be complemented by diffraction characterization.

13

The absence of the H1→M→H2 transitions can be explained by the lack of long-range lithium/vacancy ordering and collective JT distortion as a result of randomly distributed dopants[54] which disrupt the Ni^{3+} ordering. Since there is no clear explanation of the H2 → H3 transition in LNO, it remains unclear why this transition is not observed for Ni-rich NMC and NCA materials. As the potential at which the c-lattice collapse and the dQ/dV feature remains nearly unchanged at ~4.2 V vs. Li on moving from LNO to NMC-811, it is unlikely that this process has been pushed to higher potentials which are outside of the voltage window used in *operando* experiments. We speculate its absence is for the same reason as the disappearance of the monoclinic phase, i.e. disrupted lithium/vacancy ordering and collective JT distortion.

As for the H3→H4(O1) transition, no O1 phase has been reported for substituted-LNOs during electrochemical cycling, an O1 phase has been prepared via chemical delithiation for $Li_xCo_{1/3}Ni_{1/3}Mn_{1/3}O_2$ (x approaching 0)[55] Electrochemically inactive elements, for instance Al^{3+}, can prevent full delithiation of $LiTMO_2$s and therefore mitigate the H3→H4(O1) as the O3 stacking is thermodynamically more stable when the Li layers are not completely vacant.[23] In any case, as outlined above, the H3→H4(O1) transitions in LNO is predicted by DFT to be only marginally energetically favourable and is kinetically very slow, therefore the absence of an O3→O1 transition, even in materials without inactive cations (NMCs), is not that surprising. Even without the formation of a distinct O1 phase, the structure of NCA (as well as NMC111 and 532) becomes increasingly disordered along the c axis at higher SoCs (4.3 V and above for NCA), as shown by the strong anisotropies of atom displacement parameters (ADPs) values reported by Liu et al.[56] Moreover, the authors confirmed that this is mostly due to static rather than thermal displacements, as evidenced by the fact that the ADP tensor, which reflects disorder along the c direction, U33, remains large at low temperatures where thermal motion induced disorder is effectively eliminated.

Finally, we stress that the structural properties of the LNO and Ni-rich materials are highly sensitive to the synthesis conditions, for instance the amount of antisite defects, which have profound effect on the phase behaviour of these materials. This also leads to various discrepancies in the literature which show multiple phases at intermediate and/or high SoCs during initial cycles.[57,58]

5. Impacts of the structural evolution on cell performance

In this section, we review the link between the structural evolution and the degradation of the cell performance.

5.1 Bulk degradation due to structural evolution

For LNO cells, a much faster capacity fading is observed once the upper cutoff voltage is increased to 4.2 V (vs. Li) or greater. This corresponds to the onset of the H2→ H3 transition for which a massive decrease of the overall interlayer distance is observed.[59] Interestingly, although no thermodynamic two-phase regions are observed in NCA and NMC, the degradation of the cell performances is considerably accelerated particularly when using high upper cut-off voltages and the SoC regions where the c_{hex} drops substantially (for instance above 4.4 V vs. Li) are reached.[48,60–62] The explanation – at least in part – is nested in the large anisotropic lattice changes which causes both inter-granular and intra-granular cracking, which have been widely observed for Ni-rich $LiTMO_2$ materials.[62–64] Inter-granular cracking can cause losses through electrical disconnection of cathode active materials, physical loss of the cathode material into the electrolyte and creating fresh surfaces which are exposed to the electrolyte and can undergo deleterious surface reactions (involving reactions with the electrolyte and surface and subsurface structural rearrangements). Strategies for limiting the impact of this cracking have been explored, for example by infusing lithium conducting solid electrolyte into grain-boundaries to retain ionic connectivity and prevent incursion of liquid electrolyte.[65]

On the primary particle level, intragranular cracking and stacking faults are also observed particularly after high voltage cycling, which can be attributed to the strong internal mechanical stress/strain as a result of the substantial lattice contraction in the c direction, as well as other factors associated with the structural instability in the highly delithiated state (for instance, oxygen evolution).[66–69] The H3→H4(O1) transition, although rarely observed for the LNO, would be extremely detrimental to the structural stability as it requires a gliding of the transition metal slab, which is highly likely to result in the formation of stacking faults and particle fracturing, and thus poor cycling performance. Therefore, the presence a finite number of antisite defects is hypothesized to be beneficial for LNO as it can suppress the H3→H4(O1) transition.[30]

5.2 Structure reconstruction at the particle surface

We note that although this essay focuses on the bulk properties, recent studies show that the surface properties of Ni-rich material have profound impacts on their bulk structural as well as electrochemical behaviour. Therefore, we briefly review the surface-related processes here, and their influence on the bulk of the materials is discussed in detail in the following sections. First, the surface of Ni-rich materials undergoes a structural transformation from the layered to more densified structures, which were observed even just after being in contact with the electrolyte and that continue to grow upon cycling.[70] Such densified phases are proposed to possess spinel- and/or rocksalt-like structures as shown by numerous (scanning) transmission electron microscopy studies.[18,66,70,71] First principles-based kinetic Monte Carlo simulations suggest that such densified structures can be attributed to $Ni_{0.25}NiO_2$ and $Ni_{0.5}NiO_2$ type phases which are formed due to nickel back diffusion from the surface.[72] This surface reconstruction process results in a direct loss of active material and the formed surface layer can further deteriorate the cycling performance by impeding lithium and electron transport, as well as leading to bulk fatigued degradation (see section 6.2 for more discussion). It should also be noted that this structural densification process must be accompanied by lattice oxygen

release. The released oxygen, for instance, in the form of highly reactive singlet oxygen,[73] can chemically oxidize the electrolyte and result in various degradation processes. Indeed, Jung et al. demonstrated, using online electrochemical mass spectroscopy (OEMS), that oxygen is released from the surface of various NMCs and reacts with the electrolyte producing CO_2 and CO.[51] This is consistent with results showing that chemical, rather than electrochemical, oxidation is the dominant source of electrolyte oxidation at the cathode in LCO/graphite cells.[74] Indeed, the conventional $LiPF_6$- and carbonate-based electrolytes has been shown to stable to above 5 V (measured on glassy carbon[75] and $LiNi_{0.5}Mn_{1.5}O_4$ cathode[76,77]). These degradation processes are further aggravated by the intra- and inter-granular cracking discussed above, which are highly likely to expose fresh surfaces and therefore facilitate additional surface reconstruction.

Second, the surface of Ni-rich materials, in practice, is covered by a contamination layer typically composed of residues from synthesis (e.g. LiOH) and products from reactions with ambient air during storage. This surface layer can lead to non-uniform reaction kinetics and also faster capacity fading (more discussions in section 6.1).

6. Phase behaviour during cycling

We would like to remind the reader that the lithiation/delithiation of Ni-rich $LiTMO_2$ (Ni ≤ 80%) cathodes intrinsically follows solid solution mechanism; thus, only one rhombohedral phase is expected during the cycling. However, the coexistence of multiple phases has been observed during the cycle life of the material. In this next section, we will address their formation, nature and origin.

6.1 During initial cycles

A two-phase coexistence has been observed at low voltages for many Ni-rich $LiTMO_2$ compositions during their first charge.[29,48,78] The compositional range over which this transformation occurs can vary even in samples with the same nominal compositions (in

$Li_xNi_{0.8}Co_{0.15}Al_{0.05}O_2$: Robert et al. ca. 0.03 < x < 0.39, Yoon et al. ca. 0.07 < x < 0.55), which strongly suggests this is not an intrinsic property of the materials. This so called "two-phase" transition (sometimes termed H1–H2) is in fact a result of surface contaminants, which in addition to causing greater capacity fading and more challenging electrode preparation, lead to substantial kinetic barriers to Li deintercalation.[78,79] The presence of a surface layer, which is composed of some mixture of Li_2CO_3, $LiHCO_3$, $NiCO_3$ and NiO-like species,[79–81] impedes Li deintercalation and gives rise to a higher OCV and a overpotential spike. The magnitude of this overpotential varies depending on the degree and thickness of surface coverage and is conspicuously absent in samples with minimal surface species.[78,79,82]. As the (carbonate-containing) contaminants are oxidized and the layer breaks down on charging, heterogeneity in both this breakdown process and the initial coverage give raise to a non-uniform delithiation between primary particles, leading to a surface induced kinetic phase gap. Non-uniformity has been shown to persist in NCA, even after 7 days of relaxation at open circuit, further suggesting that the heterogeneity is at least between individual primary particles.[82] The heterogeneity is absent in subsequent cycles with some authors referring to the overpotential spike as part of an "activation" process,[83,84] however with careful synthesis and handling or even treatment of "exposed" samples,[80,81] this phenomenon can be mitigated. The deleterious effects of surface impurity species necessitate careful storage and cell preparation for all Ni-rich layered $LiTMO_2$ materials especially when considering their intrinsic properties.

Another, less pronounced two-phase coexistence can be observed even in samples which have been meticulously prepared to minimise surface species formation.[50]. On charging from close to full lithiation (for example, pristine material, or material discharged potentiostatically), a subtle two-phase coexistence is observed.[50] The difference in Li composition (estimated from lattice parameter changes) is lower than that for the surface induced heterogeneity discussed above. The origin of the phase gap is also kinetic, and nested

in Li mobility which is extremely poor at near complete lithiation but rises rapidly with delithiation (the fast motion regime is $x \leq 0.86$ for $Li_xNi_{0.8}Co_{0.15}Al_{0.05}O_2$ as determined by a combination of linewidth and spin-spin, T_2, relaxation NMR measurements).[50] On charge, any particles close to full lithiation have extremely slow Li kinetics and thus a large overpotential to delithiation, whereas any particles which have been slightly delithiated have much lower overpotentials and only slightly higher thermodynamic potentials to delithiation. This drives a small "kinetic" two-phase coexistence. On discharging, under normal cycling conditions, no two-phase coexistence is observed as lithiation at the concentrations where the Li kinetics becomes extremely sluggish is no longer possible. This also causes an upper cut-off voltage independent capacity loss on first cycle observed across the Ni-rich materials,[50,84–86] as well as in doped LCOs.[87–90] This capacity loss can be largely reversed by slow discharging (for example galvanostatic discharging until 2.5 V followed by potentiostatic discharging), and both long-range (lattice parameters from diffraction) and short-range (NMR shifts and lineshapes) structural parameters can return to near-pristine values.[50]

Kinetically slow processes can lead to irreversible losses, which become more severe as the cycling progresses, as well as at high rates; the latter is a very common phenomenon in lithium-ion batteries due to a non-uniform current distribution. Further kinetically induced reaction heterogeneity after extensive ageing will be discussed in the next section.

6.2 After ageing

For materials which show rapid capacity fading, both NCA[50,78,91] and NMC-811[29,49] show remarkably reversible long-range structure evolution on charge and discharge; the lattice parameters for NMC-811 cycled between 3.0 and 4.4 V show very little hysteresis between charge and discharge and excellent reversibility between first and second cycles.[29] This aligns well with the observation that degradation in Ni-rich $LiTMO_2$ cathodes is a gradual and continuous process. After prolonged electrochemical cycling, no bulk phase transformation from layered to spinel and/or rocksalt has been reported in the literature, and no obvious

increase in the antisite defects is observed after ageing at room temperature.[49,71] Moreover, the overall change in the lattice parameters as a function of SoC is in good agreement with what is observed during initial cycles, that is the *a*-parameter decreases while the *c*-parameter increases initially and then collapse at high SoCs.[49,71]

Several studies have, however, reported the observation of apparent "two-phase" reactions after extended ageing, which seems to contradict the fact that the lithiation/delithiation of Ni-rich materials are intrinsically single-phase reactions.[63,71,91,92] Liu et al. performed *operando* X-ray diffraction on an NCA ($LiNi_{0.8}Co_{0.15}Al_{0.05}O_2$) material at a fresh state (after 2 cycles) and after prolonged cycling (after 92 cycles),[63] where the ageing was carried out in a half cell (i.e. Li metal anode) at a cycling rate of 14 mA/g and a voltage window of 2.7-4.5 V. The *operando* XRD results of the second cycle confirms NCA follows a solid-solution mechanism. However, at cycle 92nd and 93rd, obvious peak broadening and splitting are observed for the (003) and (113) reflections as indicated by the arrows in Figure 3a. The authors attributed the additional phase to an NCA population which with sluggish lithiation and delithiation. Specifically, the more reactive component is active between 10% and 80% SoC (i.e. Li composition of 0.9 and 0.2, respectively) while the sluggish population can only reach a maximum SoC of ~50% as shown in Figure 3b. Phase segregations in NCA are also observed in commercial-grade cylindrical cells which were aged for 34 weeks at 50 ºC at a rate of 8C between 40 % and 80 % SoC.[91] A completely inactive NCA phase was identified by X-ray diffraction which showed that this phase had lattice parameters similar to that at fully lithiated state even when the electrode was at fully charged state.

Similar phase segregations, particularly at high SoCs, are observed in Ni-rich NMCs (NMC-811[71] and NMC-850510 ($LiNi_{0.85}Mn_{0.05}Co_{0.10}O_2$)[92]. For NMC-811 (shown in Figure 3d), the (003) peak of the NMC-811 during the first 1.5 h of the charging period at cycle 348 gradually shifts to lower angles with no obvious peak broadening or splitting, indicating that within this SoC range, the material follows the expected solid-solution behaviour.[71] In

contrast, clear peak splitting was observed on further delithiation, which was modelled with three rhombohedral phases with distinct lattice parameters – hence with different SoCs - *via* Rietveld refinement. Moreover, the phase fraction of fatigued component (i.e. at the lowest SoC) continues to increase as the cycling progresses from cycle 348 to 915 as shown in Figure 3e. These observations are in good agreement with a recent study on the ageing of NMC850510 by Schweidler et al.[92]
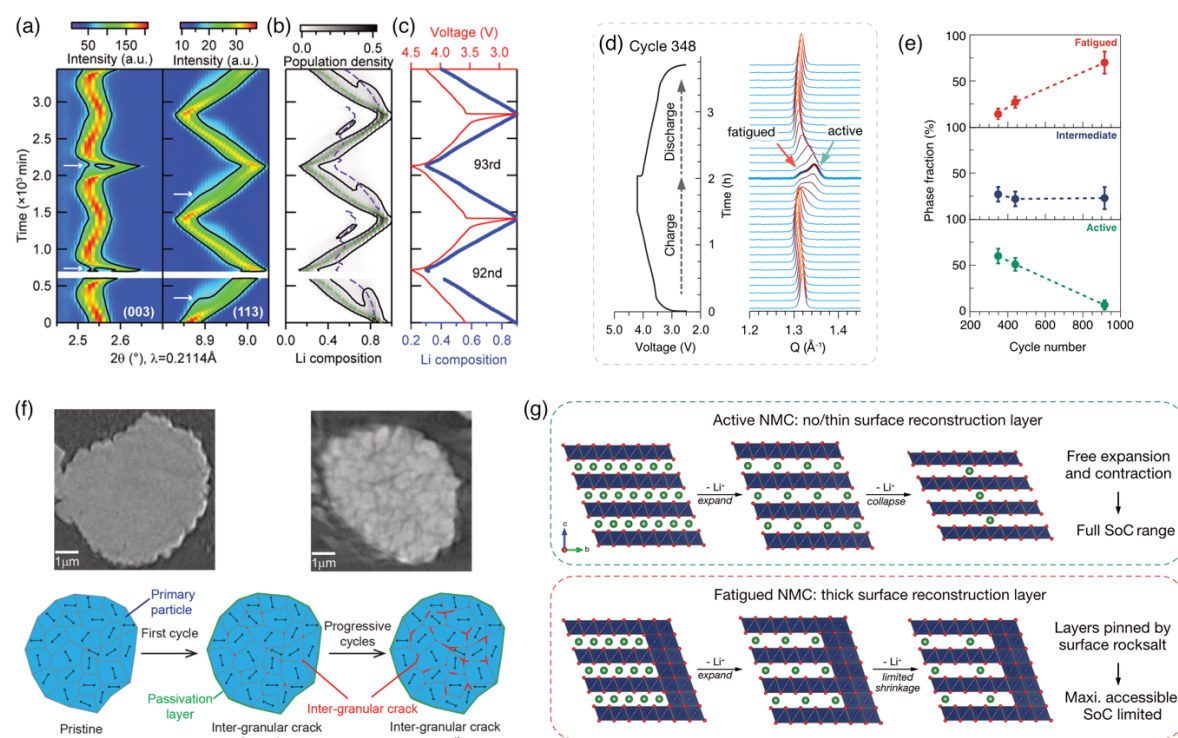

Figure 3. Phase segregation in layered Ni-rich cathodes after ageing. a,b,c) The (003) and (113) reflection of an NCA cathode (a) during the 92nd and 93rd cycles, and the corresponding population densities (i.e. phase fractions) of the active (dashed green line) and sluggish (dashed purple line) populations and their Li contents (b), and voltage profile (c). d,e) The (003) reflection of an NMC-811 cathode during cycle 348 (d) and phase fractions (e). f) Illustration of the propagation of intergranular cracking after multiple cycles. (g) Illustration of the structural evolution of the active phase and the fatigued phase during delithiation. Panels (a-c, f) reproduced with permission from reference[63]. Copyright 2019, American Chemical Society. Panels (d,e,g) reproduced with permission from reference[71]. Copyright 2020 Nature Publishing Group.

Several mechanisms have been proposed to explain the observed phase segregation in such Ni-rich materials after ageing. One possibility is that the phase segregation is a result of intergranular cracking, which leads to isolated particles as illustrated in Figure 3f.[63,91]

Industry-standard Ni-rich materials are synthesized via co-precipitation methods which produce spherical agglomerates composed of hundreds-of-nanometre sized primary particles. During the charge and discharge, the material exhibits anisotropic lattice change as discussed in the previous section, and in particular the rapid contraction in the particle size, which causes intergranular cracking. The primary particles which lose electronic and ionic conduction pathway are therefore less reactive during the cycling. Schweidler et al proposed another mechanism where the sluggish population results from a kinetic limitation as a result of cathode electrolyte interface (CEI) formation involving surface reconstruction from layered to rocksalt-like structure as well as particle fracturing.[92]

More recently, Xu et al. showed that the fatigued population still exists in single-crystal NMC charged to high SoCs with extremely slow currents, suggesting that this phenomenon cannot be explained solely by intergranular cracking and kinetic limitations. The authors found that the fatigued phases had highly similar lattice parameters – hence a similar SoC (at ~75%) – in several aged NMC-811 samples and suggested there is a structural origin behind such fatigue processes. Specifically, the fact that the lattice of bulk layered structure expands and contracts during the cycling, while that of the reconstructed surface rocksalt remains unchanged, will generate substantial lattice mismatch at the interface. Such mismatch becomes particularly pronounced when the material approaches 75% SoC due to the rapid decrease in the *c*-parameter. As a result, the bulk layered structure appears to be pinned by the surface rocksalt layer due to the strong lattice strain as illustrated in Figure 3g and the fatigued population cannot be further delithiated beyond the threshold of 75% SoC. Note that this pinning mechanism is likely to be coupled with other structural change processes at high SoCs discussed above in section 3, 4 and 5. For instance, delithiation of the NMC-811 beyond 75% SoC is associated with the voltage plateau at ~4.2 V vs Li, which is similar to the electrochemical signature reminiscent of the H2→H3 transition in LNO (Figure 1). The

material is therefore likely to be prone to this phase transition, or becomes more disordered as demonstrated for NCA at high SoCs.[56]

7. Summary and Outlook

This essay reviews recent advances in the understanding of the phase behaviour of layered LiNiO$_2$ and its analogues Ni-rich materials during electrochemical cycling. The parent material LNO exhibits a series of phase transformations of H1→M→H2→H3, whereas substituted Ni-rich NMC and NCA materials (Ni ≤ 80 %) intrinsically follow solid-solution mechanisms during cycling, despite the fact that similar voltage (dQ/dV) features, reminiscent of the various phase transitions in LNO, are still discernible. We therefore highlight that it is misleading to use such electrochemistry signatures as direct evidence for the presence of phase transformations. Both LNO and its derivates show rapid lattice contraction in the c direction at high SoCs, which leads to severe mechanical degradation.

In practice, multiple apparent "two-phase" reactions are observed during the cycling of the Ni-rich cathodes, both during initial cycling and after extensive ageing as demonstrated by several recent reports. Ni-rich cathode materials may show two "two-phase" reactions at the very beginning of the first charge, both of which are attributed to kinetically induced phase gaps that are the result of (i) a surface contaminant layer and (ii) slow lithium diffusion kinetics when the cathode material is close to full lithiation. Furthermore, phase segregations are observed after prolonged ageing which are proposed to stem from intergranular cracking, kinetic limitations as well as a new mechanism associated with the high interfacial lattice strain between the bulk layered structure and thick surface rocksalt layer at high SoCs. Despite this recent progress, due to the extremely wide range of cathode compositions and cell chemistries (full cells vs half cells, use of additives etc), as well as the difficultly in synthesizing and handling high quality Ni-rich LiTMO$_2$s, a comprehensive knowledge of the phase behaviour of Ni-rich cathodes is still lacking. In particular, the nature of the various

high voltage processes, which are undoubtedly related to the rapid performance fading when these materials are cycled with high upper cutoff voltages, must be understood in order to further the development of such state-of-the-art materials. Much of our understanding of the phase behaviour of NCA and Ni-rich NMC derives from excellent but relatively old studies of $LiNiO_2$ and with the continual improvements in operando diffraction and other advanced characterization techniques, we would urge new studies into the high voltage behavior in $LiNiO_2$, particularly the H3 phase which is particularly poorly understood. Indeed, this knowledge is essential to the understanding of the absence of H2-H3 transitions in ~80% Ni compounds, and more importantly, to the exploration of the minimum dopant content required to eliminate this detrimental transition as today's battery research and development is pushing to even higher Ni-content cathodes. Finally, we stress the importance of decoupling the intrinsic and extrinsic phase behaviours, not only for layer Ni-rich cathodes, but also other materials such as polyanionic compounds as well as those in post Li-ion technologies.

Received: ((will be filled in by the editorial staff))
Revised: ((will be filled in by the editorial staff))
Published online: ((will be filled in by the editorial staff))

References

(1) G. E. Blomgren, *J. Electrochem. Soc.* **2016**, *164*, A5019-A5025.
(2) Z. P. Cano; D. Banham; S. Ye; A. Hintennach; J. Lu; M. Fowler; Z. Chen, *Nat. Energy* **2018**, *3*, 279-289.
(3) R. Schmuch; R. Wagner; G. Hörpel; T. Placke; M. Winter, *Nat. Energy* **2018**, *3*, 267-278.
(4) J. Kim; H. Lee; H. Cha; M. Yoon; M. Park; J. Cho, *Adv. Energy Mater.* **2018**, *8*, 1702028.
(5) W. Li; E. M. Erickson; A. Manthiram, *Nat. Energy* **2020**, *5*, 26-34.
(6) J. R. Dahn; U. von Sacken; C. A. Michal, *Solid State Ionics* **1990**, *44*, 87-97.
(7) T. Ohzuku; A. Ueda; M. Nagayama, *J. Electrochem. Soc.* **1993**, *140*, 1862-1870.
(8) M. S. Whittingham, *Chem. Rev.* **2004**, *104*, 4271-4302.

(9) J. Kasnatscheew; M. Evertz; R. Kloepsch; B. Streipert; R. Wagner; I. Cekic Laskovic; M. Winter, *Energy Technology* **2017**, *5*, 1670-1679.

(10) U. S. G. Survey, Mineral Commodity Summaries 2020: Cobalt, https://pubs.usgs.gov/periodicals/mcs2020/mcs2020-cobalt.pdf, accessed: November **2020**

(11) U. S. G. Survey, Mineral Commodity Summaries 2020: Nickel, https://pubs.usgs.gov/periodicals/mcs2020/mcs2020-nickel.pdf, accessed: November **2020**

(12) M. D. Radin; S. Hy; M. Sina; C. Fang; H. Liu; J. Vinckeviciute; M. Zhang; M. S. Whittingham; Y. S. Meng; A. Van der Ven, *Adv. Energy Mater.* **2017**, *7*, 1602888.

(13) M. Z. Bazant, *Acc. Chem. Res.* **2013**, *46*, 1144-1160.

(14) W. Dreyer; J. Jamnik; C. Guhlke; R. Huth; J. Moškon; M. Gaberšček, *Nat. Mater.* **2010**, *9*, 448-453.

(15) X. Zhang; M. van Hulzen; D. P. Singh; A. Brownrigg; J. P. Wright; N. H. van Dijk; M. Wagemaker, *Nat. Commun.* **2015**, *6*, 8333.

(16) J. Lim; Y. Li; D. H. Alsem; H. So; S. C. Lee; P. Bai; D. A. Cogswell; X. Liu; N. Jin; Y. S. Yu; N. J. Salmon; D. A. Shapiro; M. Z. Bazant; T. Tyliszczak; W. C. Chueh, *Science* **2016**, *353*, 566-571.

(17) M. M. Thackeray, *Prog. Solid State Chem.* **1997**, *25*, 1-71.

(18) C. Tian; F. Lin; M. M. Doeff, *Acc. Chem. Res.* **2018**, *51*, 89-96.

(19) A. Manthiram; B. Song; W. Li, *Energy Storage Mater.* **2017**, *6*, 125-139.

(20) S.-T. Myung; F. Maglia; K.-J. Park; C. S. Yoon; P. Lamp; S.-J. Kim; Y.-K. Sun, *ACS Energy Letters* **2017**, *2*, 196-223.

(21) C. Delmas; C. Fouassier; P. Hagenmuller, *Physica B+C* **1980**, *99*, 81-85.

(22) A. Van der Ven; M. K. Aydinol; G. Ceder, *J. Electrochem. Soc.* **1998**, *145*, 2149-2155.

(23) A. Van der Ven; M. K. Aydinol; G. Ceder; G. Kresse; J. Hafner, *Phys. Rev. B* **1998**, *58*, 2975-2987.

(24) Z. Chen; Z. Lu; J. R. Dahn, *J. Electrochem. Soc.* **2002**, *149*, A1604.

(25) C. Delmas; J. P. Pérès; A. Rougier; A. Demourgues; F. Weill; A. Chadwick; M. Broussely; F. Perton; P. Biensan; P. Willmann, *J. Power Sources* **1997**, *68*, 120-125.

(26) L. Yin; Z. Li; G. S. Mattei; J. Zheng; W. Zhao; F. Omenya; C. Fang; W. Li; J. Li; Q. Xie; E. M. Erickson; J.-G. Zhang; M. S. Whittingham; Y. S. Meng; A. Manthiram; P. G. Khalifah, *Chem. Mater.* **2020**, *32*, 1002-1010.

(27) M. Bianchini; M. Roca-Ayats; P. Hartmann; T. Brezesinski; J. Janek, *Angew. Chem. Int. Ed.* **2019**, *58*, 10434-10458.

(28) L. de Biasi; A. Schiele; M. Roca-Ayats; G. Garcia; T. Brezesinski; P. Hartmann; J. Janek, *ChemSusChem* **2019**, *12*, 2240-2250.

(29) K. Märker; P. J. Reeves; C. Xu; K. J. Griffith; C. P. Grey, *Chem. Mater.* **2019**, *31*, 2545-2554.

(30) L. Croguennec; C. Pouillerie; C. Delmas, *J. Electrochem. Soc.* **2000**, *147*, 1314.

(31) H. Li; N. Zhang; J. Li; J. R. Dahn, *J. Electrochem. Soc.* **2018**, *165*, A2985-A2993.

(32) C. Delmas; M. Ménétrier; L. Croguennec; S. Levasseur; J. P. Pérès; C. Pouillerie; G. Prado; L. Fournès; F. Weill, *Int. J. Inorg. Mater.* **1999**, *1*, 11-19.

(33) W. Li; J. Reimers; J. Dahn, *Solid State Ionics* **1993**, *67*, 123-130.

(34) L. Croguennec; C. Pouillerie; A. N. Mansour; C. Delmas, *J. Mater. Chem.* **2001**, *11*, 131-141.

(35) L. Croguennec; C. Pouillerie; C. Delmas, *Solid State Ionics* **2000**, *135*, 259-266.

(36) H. Arai; S. Okada; H. Ohtsuka; M. Ichimura; J. Yamaki, *Solid State Ionics* **1995**, *80*, 261-269.

(37) J. P. Peres; F. Weill; C. Delmas, *Solid State Ionics* **1999**, *116*, 19-27.

(38) M. E. Arroyo y de Dompablo; A. Van der Ven; G. Ceder, *Phys. Rev. B* **2002**, *66*, 064112.

(39) M. E. Arroyo y de Dompablo; C. Marianetti; A. Van der Ven; G. Ceder, *Phys. Rev. B* **2001**, *63*, 144107.

(40) M. E. Arroyo y de Dompablo; G. Ceder, *J. Power Sources* **2003**, *119-121*, 654-657.

(41) M. E. Arroyo y de Dompablo; G. Ceder, *Chem. Mater.* **2003**, *15*, 63-67.

(42) D. Carlier; M. Ménétrier; C. P. Grey; C. Delmas; G. Ceder, *Phys. Rev. B* **2003**, *67*, 174103.

(43) D. S. Middlemiss; A. J. Ilott; R. J. Clément; F. C. Strobridge; C. P. Grey, *Chem. Mater.* **2013**, *25*, 1723-1734.

(44) D. Carlier; M. Ménétrier; C. Delmas, *J. Mater. Chem.* **2001**, *11*, 594-603.

(45) C. Chazel; M. Ménétrier; L. Croguennec; C. Delmas, *Inorg. Chem.* **2006**, *45*, 1184-1191.

(46) A. Manthiram; J. Choi, *J. Power Sources* **2006**, *159*, 249-253.

(47) J. Choi; A. Manthiram, *J. Mater. Chem.* **2006**, *16*, 1726-1733.

(48) J. Li; L. E. Downie; L. Ma; W. Qiu; J. R. Dahn, *J. Electrochem. Soc.* **2015**, *162*, A1401-A1408.

(49) F. Friedrich; B. Strehle; A. T. S. Freiberg; K. Kleiner; S. J. Day; C. Erk; M. Piana; H. A. Gasteiger, *J. Electrochem. Soc.* **2019**, *166*, A3760-A3774.

(50) A. Grenier; P. J. Reeves; H. Liu; I. D. Seymour; K. Märker; K. M. Wiaderek; P. J. Chupas; C. P. Grey; K. W. Chapman, *J. Am. Chem. Soc.* **2020**, *142*, 7001-7011.

(51) R. Jung; M. Metzger; F. Maglia; C. Stinner; H. A. Gasteiger, *J. Electrochem. Soc.* **2017**, *164*, A1361-A1377.

(52) S.-U. Woo; C. S. Yoon; K. Amine; I. Belharouak; Y.-K. Sun, *J. Electrochem. Soc.* **2007**, *154*, A1005.

(53) H.-J. Noh; S. Youn; C. S. Yoon; Y.-K. Sun, *J. Power Sources* **2013**, *233*, 121-130.

(54) P. Whitfield; I. Davidson; L. Cranswick; I. Swainson; P. Stephens, *Solid State Ionics* **2005**, *176*, 463-471.

(55) S.-C. Yin; Y.-H. Rho; I. Swainson; L. F. Nazar, *Chem. Mater.* **2006**, *18*, 1901-1910.

(56) H. Liu; H. Liu; I. D. Seymour; N. Chernova; K. M. Wiaderek; N. M. Trease; S. Hy; Y. Chen; K. An; M. Zhang; O. J. Borkiewicz; S. H. Lapidus; B. Qiu; Y. Xia; Z. Liu; P. J. Chupas; K. W. Chapman; M. S. Whittingham; C. P. Grey; Y. S. Meng, *J. Mater. Chem. A* **2018**, *6*, 4189-4198.

(57) C. Tian; Y. Xu; W. H. Kan; D. Sokaras; D. Nordlund; H. Shen; K. Chen; Y. Liu; M. Doeff, *ACS Appl. Mater. Interfaces* **2020**, *12*, 11643-11656.

(58) J. Alvarado; C. Wei; D. Nordlund; T. Kroll; D. Sokaras; Y. Tian; Y. Liu; M. M. Doeff, *Mater. Today* **2020**, *35*, 87-98.

(59) C. S. Yoon; D.-W. Jun; S.-T. Myung; Y.-K. Sun, *ACS Energy Letters* **2017**, *2*, 1150-1155.

(60) J. Li; J. Harlow; N. Stakheiko; N. Zhang; J. Paulsen; J. Dahn, *J. Electrochem. Soc.* **2018**, *165*, A2682-A2695.

(61) W. Li; X. Liu; Q. Xie; Y. You; M. Chi; A. Manthiram, *Chem. Mater.* **2020**,

(62) H. Li; A. Liu; N. Zhang; Y. Wang; S. Yin; H. Wu; J. R. Dahn, *Chem. Mater.* **2019**,

(63) H. Liu; M. Wolf; K. Karki; Y. S. Yu; E. A. Stach; J. Cabana; K. W. Chapman; P. J. Chupas, *Nano Lett.* **2017**, *17*, 3452-3457.

(64) P.-C. Tsai; B. Wen; M. Wolfman; M.-J. Choe; M. S. Pan; L. Su; K. Thornton; J. Cabana; Y.-M. Chiang, *Energy Environ. Sci.* **2018**, *11*, 860-871.

(65) P. Yan; J. Zheng; J. Liu; B. Wang; X. Cheng; Y. Zhang; X. Sun; C. Wang; J.-G. Zhang, *Nat. Energy* **2018**, *3*, 600-605.

(66) S. Ahmed; A. Pokle; S. Schweidler; A. Beyer; M. Bianchini; F. Walther; A. Mazilkin; P. Hartmann; T. Brezesinski; J. Janek; K. Volz, *ACS Nano* **2019**,

(67) P. Yan; J. Zheng; M. Gu; J. Xiao; J. G. Zhang; C. M. Wang, *Nat. Commun.* **2017**, *8*, 14101.

(68) P. Yan; J. Zheng; T. Chen; L. Luo; Y. Jiang; K. Wang; M. Sui; J.-G. Zhang; S. Zhang; C. Wang, *Nat. Commun.* **2018**, *9*, 2437.

(69) M. D. Radin; J. Alvarado; Y. S. Meng; A. Van der Ven, *Nano Letters* *Nano Lett.* **2017**, *17*, 7789-7795.

(70) F. Lin; I. M. Markus; D. Nordlund; T.-C. Weng; M. D. Asta; H. L. Xin; M. M. Doeff, *Nat. Commun.* **2014**, *5*, 3529.

(71) C. Xu; K. Märker; J. Lee; A. Mahadevegowda; P. J. Reeves; S. J. Day; M. F. Groh; S. P. Emge; C. Ducati; B. Layla Mehdi; C. C. Tang; C. P. Grey, *Nat. Mater.* **2020**,

(72) P. Xiao; T. Shi; W. Huang; G. Ceder, *ACS Energy Letters* **2019**, *4*, 811-818.

(73) J. Wandt; A. T. S. Freiberg; A. Ogrodnik; H. A. Gasteiger, *Mater. Today* **2018**, *21*, 825-833.

(74) B. L. D. Rinkel; D. S. Hall; I. Temprano; C. P. Grey, *J. Am. Chem. Soc.* **2020**, *142*, 15058-15074.

(75) X. Kang; P. D. Sheng; R. J. T., *J. Electrochem. Soc.* **1999**, *146*, 4172-4178.

(76) J. Kasnatscheew; B. Streipert; S. Röser; R. Wagner; I. Cekic Laskovic; M. Winter, *Phys. Chem. Chem. Phys.* **2017**, *19*, 16078-16086.

(77) B. Streipert; L. Stolz; G. Homann; P. Janßen; I. Cekic-Laskovic; M. Winter; J. Kasnatscheew, *ChemSusChem* **2020**, *13*, 5301-5307.

(78) A. Grenier; H. Liu; K. M. Wiaderek; Z. W. Lebens-Higgins; O. J. Borkiewicz; L. F. J. Piper; P. J. Chupas; K. W. Chapman, *Chem. Mater.* **2017**, *29*, 7345-7352.

(79) R. Jung; R. Morasch; P. Karayaylali; K. Phillips; F. Maglia; C. Stinner; Y. Shao-Horn; H. A. Gasteiger, *J. Electrochem. Soc.* **2018**, *165*, A132-A141.

(80) J. Sicklinger; M. Metzger; H. Beyer; D. Pritzl; H. A. Gasteiger, *J. Electrochem. Soc.* **2019**, *166*, A2322-A2335.

(81) N. V. Faenza; L. Bruce; Z. W. Lebens-Higgins; I. Plitz; N. Pereira; L. F. J. Piper; G. G. Amatucci, *J. Electrochem. Soc.* **2017**, *164*, A3727-A3741.

(82) G. V. Zhuang; G. Chen; J. Shim; X. Song; P. N. Ross; T. J. Richardson, *J. Power Sources* **2004**, *134*, 293-297.

(83) X. Q. Yang; X. Sun; J. McBreen, *Electrochem. Commun.* **1999**, *1*, 227-232.

(84) R. Robert; C. Bünzli; E. J. Berg; P. Novák, *Chem. Mater.* **2015**, *27*, 526-536.

(85) H. Zhou; F. Xin; B. Pei; M. S. Whittingham, *ACS Energy Letters* **2019**, *4*, 1902-1906.

(86) J. Kasnatscheew; M. Evertz; B. Streipert; R. Wagner; R. Klöpsch; B. Vortmann; H. Hahn; S. Nowak; M. Amereller; A.-C. Gentschev; P. Lamp; M. Winter, *Phys. Chem. Chem. Phys.* **2016**, *18*, 3956-3965.

(87) Y. Jin; S. Xu; Z. Li; K. Xu; W. Ding; J. Song; H. Wang; J. Zhao, *J. Electrochem. Soc.* **2018**, *165*, A2267-A2273.

(88) N. V. Faenza; N. Pereira; D. M. Halat; J. Vinckeviciute; L. Bruce; M. D. Radin; P. Mukherjee; F. Badway; A. Halajko; F. Cosandey; C. P. Grey; A. Van der Ven; G. G. Amatucci, *Chem. Mater.* **2018**, *30*, 7545-7574.

(89) H. Kobayashi; H. Shigemura; M. Tabuchi; H. Sakaebe; K. Ado; H. Kageyama; A. Hirano; R. Kanno; M. Wakita; S. Morimoto; S. Nasu, *J. Electrochem. Soc.* **2000**, *147*, 960.

(90) M. Zou; M. Yoshio; S. Gopukumar; J.-i. Yamaki, *Chem. Mater.* **2003**, *15*, 4699-4702.

(91) K. Kleiner; D. Dixon; P. Jakes; J. Melke; M. Yavuz; C. Roth; K. Nikolowski; V. Liebau; H. Ehrenberg, *J. Power Sources* **2015**, *273*, 70-82.

(92) S. Schweidler; L. de Biasi; G. Garcia; A. Mazilkin; P. Hartmann; T. Brezesinski; J. Janek, *ACS Appl. Energy Mater.* **2019**, *2*, 7375-7384.

Biographies and photographs
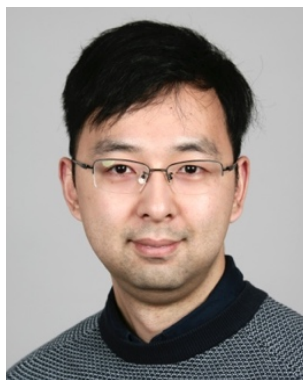
Chao Xu received his B.E. (2010) from Nanjing University of Science and Technology and M.S. (2012) and Ph.D. (2017) in Materials Chemistry from Uppsala University. He is currently a postdoc research associate at the University of Cambridge. His research focuses on high energy-density Li-ion and post Li-ion battery chemistries and advanced synchrotron characterisation techniques.

Philip J. Reeves received his MSci in Chemistry from University College London and his PhD in Chemistry from the University of Cambridge. He is currently a post-doctoral research associate at the University of Cambridge. His research focuses on understanding structure-property relationships in battery materials, especially probing the role of local structure using solid-state NMR spectroscopy.


Quentin Jacquet is a postdoctoral research associate at the University of Cambridge. He studied chemistry at Chimie Paristech, material engineering at the Universidade de Sao Paulo, and completed his PhD at the Collège de France under the supervision of Prof. Jean-Marie Tarascon. His research interests are focused on structural characterisation and crystallochemistry of electrode materials for Li-ion batteries.

Clare P. Grey is the Geoffrey-Moorhouse-Gibson and Royal Society Professor of Chemistry at Cambridge University. After receiving a BA and D. Phil. from Oxford University she was a post-doctoral fellow at Nijmegen and at DuPont CR&D. She joined Stony Brook University in 1994, moving to Cambridge in 2009, maintaining an adjunct Professorship at Stony Brook. She is a Fellow of the Royal Society and a foreign member of the American Academy of Arts and Sciences. Her current research interests include the use of solid-state NMR and diffraction-based methods to determine structure-function relationships in materials for energy storage and conversion.

Table of contents

Chao Xu, Philip J. Reeves, Quentin Jacquet, and Clare P. Grey*

Phase behaviours during electrochemical cycling of Ni-rich cathode materials for Li-ion batteries
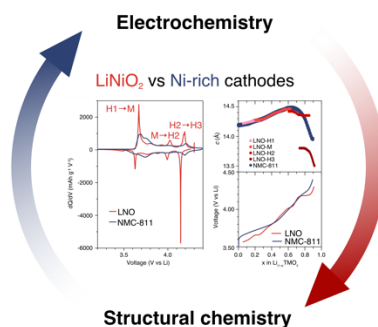
This Essay discusses the intrinsic and extrinsic phase behaviors of the state-of-the-art cathode materials, namely Ni-rich layered lithium transition metal oxides, during electrochemical cycling. We perform a close comparison with their parent material $LiNiO_2$ to highlight their similarities as well as differences in the structural properties and electrochemistry.